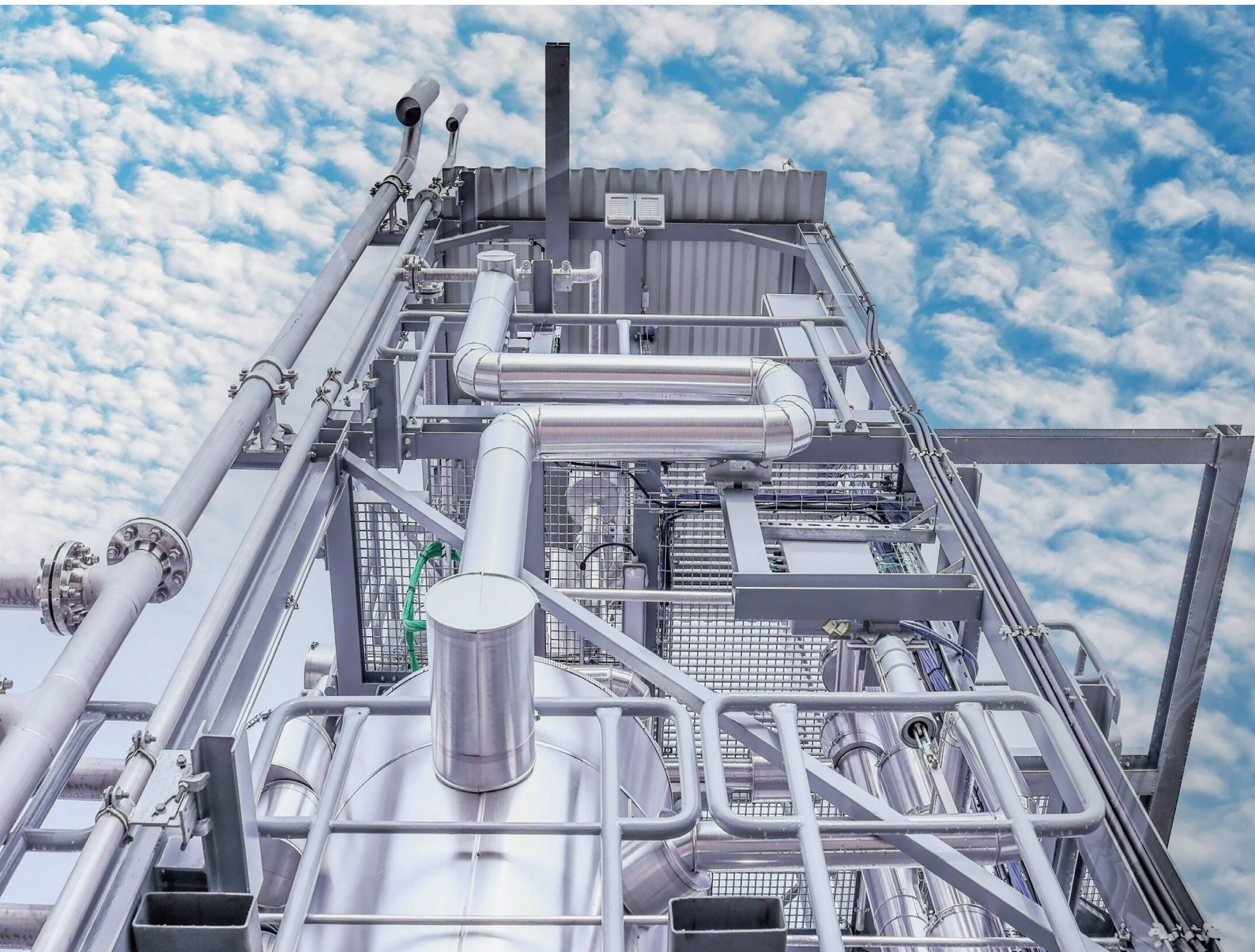


# Energy Advances

Volume 3  
Number 1  
January 2024  
Pages 1-332

[rsc.li/energy-advances](https://rsc.li/energy-advances)



ISSN 2753-1457




## PAPER

Emanuele Moioli *et al.*  
Results from the operation of an efficient and flexible  
large-scale biogas methanation system

Cite this: *Energy Adv.*, 2024,  
3, 131

# Results from the operation of an efficient and flexible large-scale biogas methanation system

Emanuele Moioli, \* Patrick Senn, Simon Østrup and Christoph Hütter

This study reports the design and operation of a power-to-gas system producing 240 kW of synthetic natural gas (SNG) from biogas and PV electricity. The system is composed of a solar field, an electrolyser, a plate-type heat exchanger methanation reactor and the required ancillary units. Biogas is cleaned from undesired components (such as H<sub>2</sub>S) and the raw gas including methane and CO<sub>2</sub> is directly processed in the reactor. The process consumes biogas and renewable electricity to produce SNG and high-pressure steam from the methanation waste heat. The process efficiency in this configuration is 76%. The methanation reactor produces grid compliant SNG in all the load cases tested and in all the biogas composition cases. The reactor shows an excellent flexibility at the start-up, as grid-compliant SNG is produced in less than 10 minutes from feed start in hot-standby. Additionally, the reactor adapts in few minutes to load changes. The reactor is modelled to better understand the origin of the excellent performance in the biogas methanation reaction. It was found that the plate-type heat exchanger operated with boiling water as cooling is an ideal solution for the methanation reaction as it approximates well the optimal reaction pathway in terms of temperature and conversion profile. Large cooling is available where needed, preventing the operation at too high temperature. Isothermal conditions are established at the end of the reactor, allowing reaching the required high conversion.

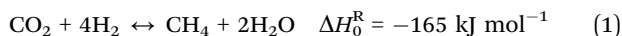
Received 1st September 2023,  
Accepted 4th November 2023

DOI: 10.1039/d3ya00436h

rsc.li/energy-advances

## 1. Introduction

The substitution of fossil-based natural gas with renewably produced synthetic methane is gaining progressively the interest of gas suppliers and policy makers due to the need of decreasing the carbon footprint of the energy supply and industry. Additionally, synthetic methane can be produced from local resources, diminishing the dependence from energy import by utilising the existing storage facilities.<sup>1</sup> This appears as a highly desirable option to stabilise the energy system against the risk of international political crises. A possible approach to produce synthetic natural gas (SNG) employs the so-called CO<sub>2</sub> methanation (or Sabatier) reaction:



The reaction recycles a low-value compound (CO<sub>2</sub>) and allows the storage of (renewably produced) H<sub>2</sub>. The process can be used to balance seasonal disparities between the energy production from renewable resources and the energy demand.<sup>2</sup>

The main hurdle for the introduction of renewable gas in the energy system is its high cost. The cost of renewable H<sub>2</sub> depends on the cost of electricity, which makes this raw material available at low cost only for limited time during the

year.<sup>3</sup> For this reason, the cost of the other reactant (CO<sub>2</sub>) should be low and preferentially negative.<sup>4</sup> In the absence of clear legislation providing an income for the plants recycling CO<sub>2</sub>, relatively few CO<sub>2</sub> sources are sufficiently economical to allow the production of cost competitive SNG.<sup>5</sup> One possible cheap CO<sub>2</sub> source is biogas. Biogas is a mixture of CO<sub>2</sub> and CH<sub>4</sub>, containing high amounts of CO<sub>2</sub> (normally between 30–50%). Currently, one popular biogas valorisation process is biogas upgrading.<sup>6</sup> This is operated by removing CO<sub>2</sub> from biogas to obtain a gas suitable for injection in the natural gas grid.<sup>7</sup> The most used technologies to this scope are scrubbers and membranes.<sup>8</sup> A new trend in the biogas use is its direct utilisation in the CO<sub>2</sub> methanation reaction. In this way, one can produce SNG without the need of prior CO<sub>2</sub> separation from biogas, obtaining low-cost CO<sub>2</sub> and receiving an additional income from the sale of the CH<sub>4</sub> contained in biogas together with the synthesized fuel.<sup>9</sup> As a drawback, the direct biogas methanation brings additional challenges compared to the standard CO<sub>2</sub> methanation, mainly connected to the necessity of removing impurities from biogas (such as H<sub>2</sub>S and organic compounds).<sup>10</sup>

Several studies showed the techno-economic feasibility of the direct biogas methanation, which can be operated both catalytically over several metallic catalysts and *via* biological processes.<sup>9,11–17</sup> However, just a few plants operated the reaction on site at a reasonable size, while more studies report

Hitachi Zosen Inova AG, Hardturmstrasse 127, CH-8005 Zurich, Switzerland.  
E-mail: Emanuele.moioli@hz-inova.com





about the methanation of biogas-derived  $\text{CO}_2$  (*i.e.*, after upgrading).<sup>18–20</sup> Specht *et al.*<sup>21</sup> showed the performance of two tubular fixed bed reactors with intermediate condensation, producing *ca.* 14 kW of SNG. Dannesboe *et al.*<sup>22</sup> operated a similar system composed of two fixed bed reactors with intermediate condensation, obtaining up to 45 kW of SNG. Witte *et al.*<sup>23</sup> reported the performance of a bubbling fluidised-bed reactor for the biogas methanation reaction, producing up to 9 kW of grid-compliant SNG after upgrading with membranes. Guilera *et al.*<sup>24</sup> showed the feasibility of the biogas methanation in microstructured heat exchanger reactors with intermediate condensation, obtaining *ca.* 15 kW of SNG. Some examples of biological methanation reactors are also available in literature, reaching larger SNG output values. Heller *et al.*<sup>25</sup> exhibited the production of SNG from biogas in a stirred bubble column operated with mixed micro-organisms, with a total production of 165 kW SNG without need of upgrading after the reactor. Hafenbradl<sup>26</sup> reported the production of 550 kW of SNG in a stirred bubble column reactor with specific archaea. Recently, a biological methanation reactor with a total installed productivity of *ca.* 1 MW SNG was inaugurated in Dietikon (CH).<sup>27</sup>

In the present study, we report the design and operation of a biogas methanation system with an SNG output of *ca.* 240 kW. As of today, at the best of our knowledge, this is the largest application of catalytic methanation in this field. The reactor operates the direct biogas methanation with the Hitachi Zosen Inova proprietary plate-type technology. The plate-type heat exchanger methanation reactor is an highly efficient reactor for the  $\text{CO}_2$  methanation, as demonstrated by several modelling and experimental studies.<sup>21,28–30</sup> This excellent performance is due to the large cooling surface area, which ensures an adequate cooling rate, essential to avoid operation in a heat transfer controlled regime.<sup>31</sup> Here, we report how the geometry and control logic of the reactor allow producing SNG from biogas,

**Table 1** Composition of biogas prior and after cleaning (ND = not detected)

Component	Raw biogas	Cleaned biogas
$\text{CH}_4$	45–55%	As raw biogas
$\text{CO}_2$	45–55%	As raw biogas
$\text{H}_2\text{S}$	140–200 ppm	ND
VOC	5–10 ppm	ND

which can be directly injected in the local natural gas grid. Furthermore, we highlight that the reactor can be operated by taking advantage of a natural draft cooling system, which reduces to a minimum the additional utilities requirement (*e.g.*, not needing coolant circulation pumps). We show how these features influence the PtG process efficiency and the dynamics of operation of the reactor. In the last section of the study, we compare the experimental results with an appropriate reactor model, drawing conclusions regarding the potential for further optimisation of the system.

## 2. Material and methods

### 2.1. System description

**Renewable gas field configuration.** The renewable gas field is located in Gabersdorf, Austria. The main components of the system are summarised in Fig. 1. At the location, a biogas plant processing agricultural waste through a wet anaerobic digestion process is present. From this biogas production, *ca.*  $22 \text{ N m}^3 \text{ h}^{-1}$  of raw biogas are fed into the methanation system. Biogas is available at room temperature and ambient pressure. The typical biogas composition is summarised in Table 1. The  $\text{CO}_2 : \text{CH}_4$  ratio is normally approximately 1 : 1 vol/vol with  $\pm 5\%$  oscillations possible. No biogas upgrading is performed in the plant. The raw biogas contains significant amounts of  $\text{H}_2\text{S}$

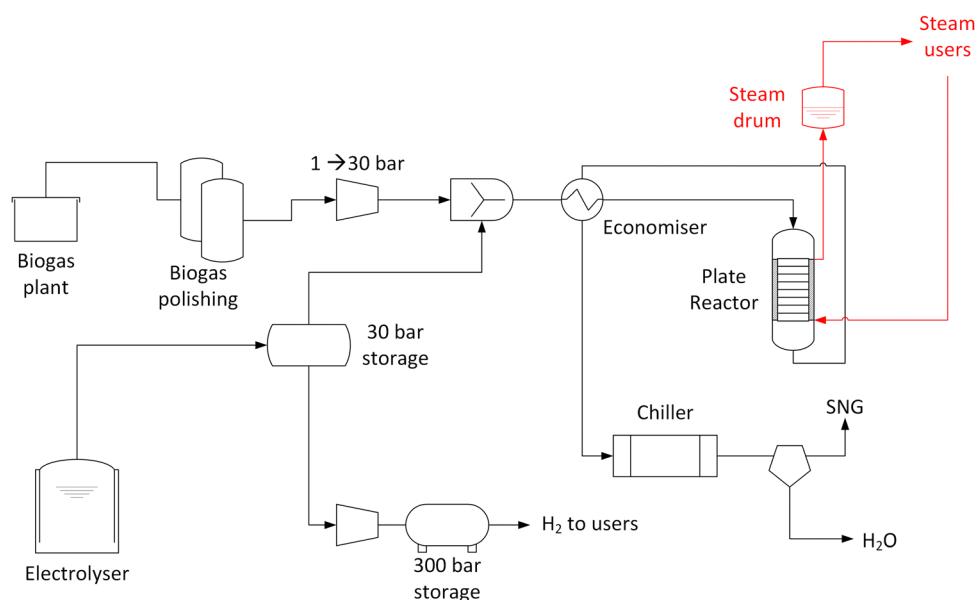


**Fig. 1** Schematic representation of the installed biogas methanation plant.





temperature is set to zero:

$$\frac{\partial^2 c_{g,i}}{\partial x^2} = 0 \quad (6)$$

$$\frac{\partial^2 T_g}{\partial x^2} = 0 \quad (7)$$

The change in flow velocity is accounted for with the continuity equation:

$$u = u^0 \cdot \frac{\rho_g^0}{\rho_g} \quad (8)$$

To simplify the resolution of the balances, the gradients inside the catalyst pellet are not calculated. This constitutes a strong limitation of the model, because of the high exothermicity of the reaction. However, the limitations in the catalyst utilisation were calculated with the Thiele modulus approach:

$$\phi = \frac{V_p}{S_p} \sqrt{\frac{n+1}{2} \cdot \left( \frac{k c_{i,s}^{n-1}}{D} \right)} \quad (10)$$

$$\eta = \frac{3}{\phi^2} (\phi \coth(\phi) - 1) \quad (11)$$

The solid balance equations are:

$$\sum_{j=1}^{NR} \eta \rho_s \nu_{ij} R_j + K_{GS} \cdot a_v \cdot (c_{g,i}^0 - c_{g,i}) = 0 \quad (12)$$

$$\sum_{j=1}^{NR} \rho_s (-\Delta H_j^R) \eta R_j + H_{GS} \cdot a_v \cdot (T_g - T_s) = 0 \quad (13)$$

The cooling medium is considered isothermal, as verified in the experimental results.

**Kinetics and correlations.** The kinetic model used for the simulations is derived from Koschany *et al.*<sup>35</sup> Although the model was originally developed for Ni/Al<sub>2</sub>O<sub>3</sub>, it was observed that this can satisfactorily describe the performance of the catalyst used in this study. The methanation reaction rate is expressed as:

$$r_{\text{Sab}} = \frac{k P_{\text{H}_2\text{O}}^{0.5} P_{\text{CO}_2}^{0.5} \left\{ 1 - \frac{P_{\text{CH}_4} P_{\text{H}_2\text{O}}^2}{P_{\text{CO}_2} P_{\text{H}_2}^4 K_{\text{eq}}} \right\}}{\left( 1 + \frac{K_{\text{OH}} P_{\text{H}_2\text{O}}}{P_{\text{H}_2}^{0.5}} + K_{\text{H}_2} P_{\text{H}_2}^{0.5} + K_{\text{mix}} P_{\text{CO}_2}^{0.5} \right)^2} \quad (14)$$

To account for the (limited) CO formation in the hotspot, the model is complemented with the RWGS rate equation by Xu and Froment,<sup>36</sup> which correctly incorporates the thermodynamic equilibrium of CO formation:

$$r_{\text{WGS}} = \frac{\frac{k_{\text{WGS}}}{P_{\text{H}_2}} \left\{ P_{\text{CO}} P_{\text{H}_2\text{O}} - \frac{P_{\text{H}_2} P_{\text{CO}_2}}{K_{\text{eq,WGS}}} \right\}}{\left( 1 + \frac{K_{\text{OH}} P_{\text{H}_2\text{O}}}{P_{\text{H}_2}^{0.5}} + K_{\text{H}_2} P_{\text{H}_2}^{0.5} + K_{\text{mix}} P_{\text{CO}_2}^{0.5} \right)^2} \quad (15)$$

The kinetics of Xu and Froment were used by changing the denominator term with the term of the Koschany kinetics. This

was done to account for the same adsorption behaviour in both reactions. As the WGS reaction is practically at equilibrium, this change has minimum influence on the calculated reaction rate. All the kinetic expressions are used without correction factors. The kinetic expressions are relevant only for the data points until the maximum temperature, after which the reactor operates in heat transfer regime. For this reason, an appropriate modelling of the heat transfer is essential for this class of reactors. The heat transfer towards the cooling medium is calculated with the analogy of resistances in series, accounting for the heat transport in the reactive medium, the wall resistance, and the cooling medium:

$$\frac{1}{h_{\text{ov}}} = \frac{1}{U_{\text{re}}} + k_w + \frac{1}{U_{\text{st}}} \quad (16)$$

The heat transfer coefficient in the reactive medium is calculated as:

$$U_{\text{re}} = \text{Nu} \cdot \frac{\lambda_g}{D} \quad (17)$$

The Nusselt number is calculated as:

$$\text{Nu} = 2 + 1.1 \cdot \text{Pr}^{\frac{1}{3}} \cdot \text{Re}^{0.6} \quad (18)$$

The heat transfer coefficient in the boiling water is set constant to 2000 kW m<sup>-2</sup> K<sup>-1</sup>.

The convective transfer between gas and catalyst is calculated as:

$$H_{\text{GS}} = k_w + 0.0029 \cdot \text{Pe}/d_p \quad (19)$$

The CO<sub>2</sub> conversion is calculated as:

$$X_{\text{CO}_2} = \frac{F_{\text{CO}_2}^0 - F_{\text{CO}_2}^{\text{out}}}{F_{\text{CO}_2}^0} \quad (20)$$

Methane yield is calculated as:

$$Y_{\text{CH}_4} = \frac{F_{\text{CH}_4}^{\text{out}}}{F_{\text{CO}_2}^0} \quad (21)$$

Efficiency is calculated as:

$$\eta_{\text{prod}} = \frac{\text{HHV}_{\text{prod}}}{\text{HHV}_{\text{in}} + P_{\text{el}}} \quad (22)$$

The model equations are implemented and solved in OpenModelica v1.18.0 (64-bit).

## 3. Results and discussion

### 3.1. Results from the reactor operation

In a normal operation procedure, the reactor is first warmed up through the start-up heater. This progressively increases the temperature of the water in the cooling system, so that the reactor is heated by direct exchange from the water/steam cycle. The start-up is operated with the reactor filled by N<sub>2</sub>. The duration of the start-up phase (*i.e.*, from cold standby to hot standby) depends on the power of the start-up heater. Hence, there is a trade-off between the CAPEX of the installed start-up heater and the time required for the cold start-up. Once the









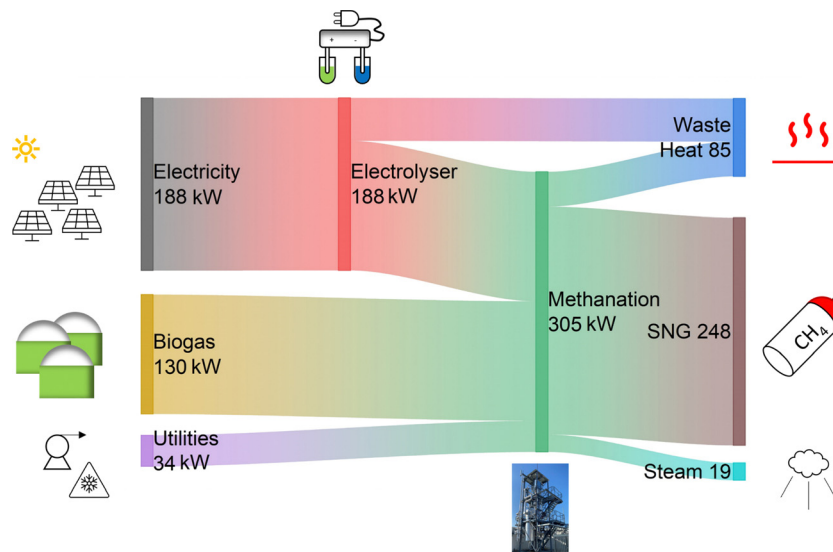


Fig. 6 Energy balance of the biogas methanation plant.

mainly to minimize the CAPEX of the heating/cooling circuit. However, part of this heat may still be usable, as the outlet temperature from the economiser is *ca.* 150 °C. In particular, the condensation heat of the product water is not used here, even though this would correspond to approximately 7 kW at a temperature above 100 °C. The Sankey diagram allows calculating the process efficiencies, which are summarised in Table 3. The feed to SNG efficiency is *ca.* 70%, resulting from the averaging of biogas upgrading and CO<sub>2</sub> conversion with H<sub>2</sub>. When steam is added in the product count, the efficiency increases to *ca.* 76%. In case an efficient use of the waste heat is envisaged (*e.g.* coupling with the biogas plant), the efficiency may rise to 79%, which is the target efficiency value of this PtG plant. These values locate the efficiency of renewable gas field in the upper limit of plants for biogas upgrading *via* PtG.<sup>4,39</sup>

### 3.2. Dynamics of the reactor

Thanks to the multipoint thermocouple inserted in one channel of the reactor, it is possible to record the temperature profile with high time and space resolution. The thermocouple covers the entire reactor, with 18 measurement points. The measurement points are not equally spaced, to improve the analysis of the reaction hotspot. The minimum spacing between two points is 20 mm, while the maximum spacing (end of the reactor) is 300 mm. The temperature profile during start-up of the reactor with the procedure described above (CO<sub>2</sub>

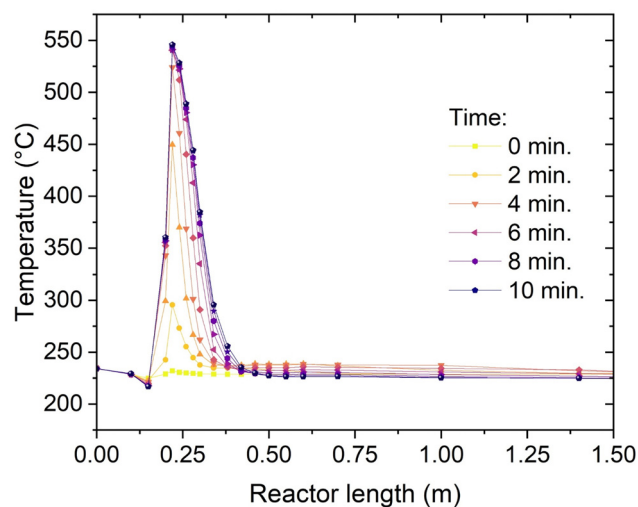


Fig. 7 Temperature profile at the start-up (experimental conditions: 8 bar, H<sub>2</sub>:CO<sub>2</sub> = 4.15, cooling set point = 230 °C).

feed start in H<sub>2</sub> atmosphere, 50% load) is shown in Fig. 7. Initially, the reactor is in hot standby, which means that the entire catalyst bed is kept at 230 °C by steam generated in the start-up heater. The feed gas at the reactor inlet is slightly colder than 200 °C, so that the temperature decreases by convective cooling in the immediate entrance of the reactor, as visible in the second and third point from the left in Fig. 7. At the start of the CO<sub>2</sub> feed, the reaction starts almost immediately, but the conversion is low, and a limited hotspot is formed (*ca.* 70 °C). The gas is quickly cooled down and the reaction proceeds with low reaction rate until the reactor outlet. This low conversion regime continues for approximately two minutes. After this time, the critical conditions for the sudden increase of the reaction rate are reached (parametric sensitivity<sup>40,41</sup>). The parametric sensitivity refers to the large change in the response

Table 3 The calculated process efficiencies

Item	Efficiency [%]
Electrolysis <sup>33</sup>	75
Feed to biomethane	70
Feed to products (incl. steam)	76
Feed to products (target) <sup>a</sup>	79

<sup>a</sup> Including complete heat utilization.







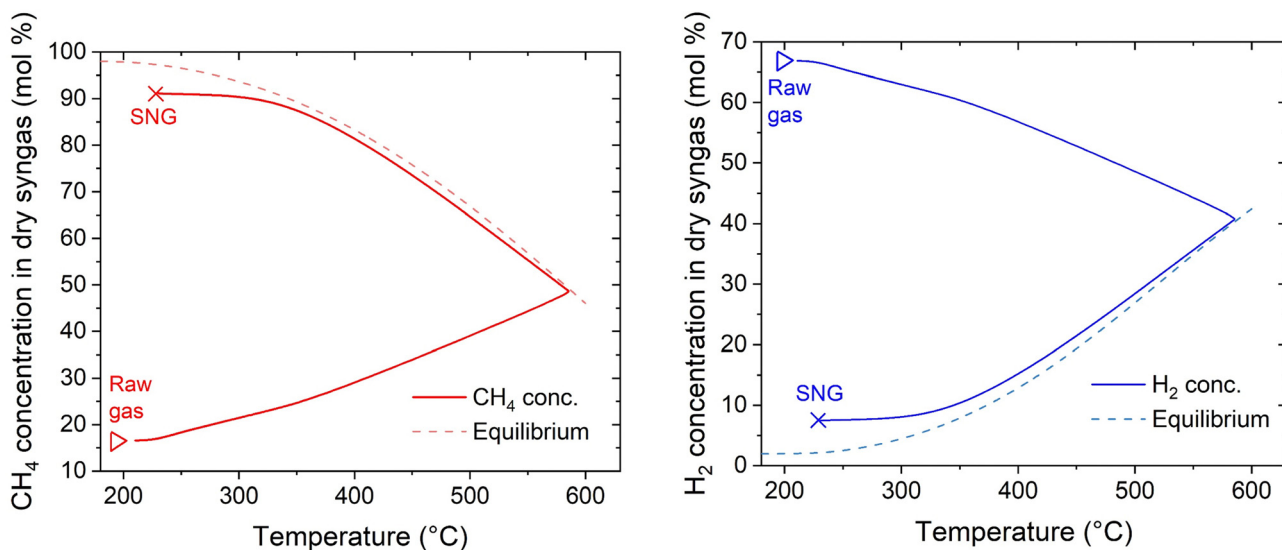


Fig. 10 Calculated concentration profiles in the reactor as a function of temperature (experimental conditions: 8 bar, H<sub>2</sub>:CO<sub>2</sub> = 4.15, CO<sub>2</sub>:CH<sub>4</sub> = 1:1, cooling setpoint = 230 °C, load = 100%).

This is confirmed by the parity plot shown in Fig. 9, where almost all the points lie in the  $\pm 10\%$  interval. The most critical points are at the reaction initiation, where the model underestimates the temperature. This is due to the difficulty in predicting the reaction activation in conditions of strong parametric sensitivity. Furthermore, the kinetic model here utilised is not tailored to the catalyst employed, hence the discrepancy can be ascribed to this factor. The temperature in the hotspot is also slightly overestimated. In this case, the discrepancy may be due to the uncertainty in the temperature management, as the temperature of the gas and of the solid is predicted as significantly different (the solid is *ca.* 20 °C hotter than the gas). The uncertainty lies in the unclear temperature measured by the thermocouple, whether it is ascribed to the solid or to the gas phase. Additionally, the conductivity effect of the thermocouple is not considered in the model here employed. The cooling section is instead well interpreted by the model, hinting that the cooling process could follow the proposed mechanism. In this section, the reaction is controlled by cooling, therefore the description of the cooling mechanism is rate determining and the influence of the kinetic model used is less relevant. This is also made evident in the insert of Fig. 5, where the methane formation rate is reported. After the hotspot, the reaction rate drops to low values, coherently with the assumption of equilibrium controlled reaction. The different extent of the hotspot is also well interpreted by the model, suggesting that the reactor operates exactly with the proposed cooling mechanism.

Further insights into the reactor properties can be retrieved by analysing the calculated concentration profiles in the reactor. These are shown in Fig. 10. The curves follow typical profiles for the methanation reactor, like reported in literature.<sup>31,44,45</sup> Starting from the inlet conditions, one can observe an initial zone where the temperature increases without significant methane production until approximately 350 °C. After this threshold,

the reaction rate increases together with the temperature. The temperature increase follows a typical runaway profile, causing the reaction hotspot. The extension of the hotspot is controlled by the reach of thermodynamic equilibrium, which is at *ca.* 570 °C and 50% CH<sub>4</sub> concentration in the dry gas. After the hotspot, the cooling is sufficient to decrease the temperature below the thermodynamic equilibrium line, hence maximising the reaction rate.<sup>42,46</sup> This allows minimising the amount of catalyst needed to reach the target conversion, attaining the 90% CH<sub>4</sub> content in the dry SNG at 300 °C after approximately 500 mm from the reactor inlet. From these results, one can deduce that the change in the extension of the hotspot is determined by the interplay of convective heat transfer and the heat produced. With increasing flow rate, the slope of the initial curve decreases, because the heat production is higher. Hence, the reach of the thermodynamic equilibrium line occurs at higher temperature and lower conversion. However, the increased heat production is balanced by the higher extent of convective heat transfer, so that the increase in the hotspot temperature is limited. Independently from the gas load at the reactor inlet, isothermal conditions are established in the second half of the reactor, allowing reaching high CO<sub>2</sub> conversion. One can therefore conclude that the plate type heat exchanger reactor, cooled with boiling water, is an excellent solution for the methanation reaction, because it ensures the most suitable cooling conditions in a large set of experimental conditions.

## 4. Conclusions

In this study, we presented selected results from the operation of a large-scale power-to-gas system, composed of a PV field, an electrolyser and a methanation reactor to produce synthetic natural gas from biogas. The system is designed to inject *ca.* 240 kW of SNG in the natural gas grid. The process produced



grid compliant SNG in all the conditions tested and showed an excellent flexibility in terms of load changes. The plate-type methanation reactor could produce *ca.* 19 kW of high-pressure steam from the cooling system, bringing the inlet to valuable products efficiency to 76%.

It was demonstrated that the system can be directly operated from biogas with a limited amount of gas cleaning, hence showing that this type of system can help increasing the production of renewable gas maximising the utilisation of biogas and operating an effective coupling with other renewable resources (in this case PV electricity). The high efficiency of the system is a promising result envisaging the possibility of retrofitting biogas plant with this technology, to maximise the productivity of the process. The reactor can adapt to oscillations in the availability of the reactants, producing compliant SNG at loads between 50–100%, without decrease in the efficiency or in the quality of the product gas. The hot-standby to steady-state time is approximately 10 minutes, which makes the system highly flexible with respect to possible shortage of H<sub>2</sub>. The special design of the methanation reactor allows limiting the reaction hotspot below 600 °C, hence limiting the risk of catalyst deactivation by coking or sintering. The modelling results showed that the combination of large cooling surface and use of boiling water as cooling medium is the essential element allowing the maximisation of the reactor performance by optimising the heat exchange. The large cooling avoids operating at too high temperature, preventing damages to the catalyst. The cooling with boiling water allows reaching isothermal conditions in the second half of the reactor, ensuring the required high conversion.

According to the results presented in this study, the existing configuration of the 'renewable gasfield' is an ideal solution to ensure a maximal utilisation the renewable resources, allowing a reliable and flexible production of local sustainable gas. The plant could be easily replicated or scaled up according to the need of different biogas sites. An extensive application of the concept here presented could represent a ready to implement solution to substantially increase the production of renewable gas, contributing to the energetic autarchy and to the reduction of the CO<sub>2</sub> footprint of natural gas users.

## Author contributions

Emanuele Moiola: conceptualization, methodology, investigation, formal analysis, data curation, writing – original draft, writing – review & editing. Patrick Senn: conceptualization, methodology, investigation, writing – review & editing. Simon Østrup: conceptualization, investigation, writing – review & editing. Christoph Hütter: conceptualization, methodology, investigation, validation, supervision, funding acquisition.

## Data availability

Data will be made available upon reasonable request.

## List of symbols

### Small letters

$a_v$	Specific surface [m <sup>-1</sup> ]
$c_i$	Concentration of the species $i$ [mol m <sup>-3</sup> ]
$c_p$	Specific heat [J mol <sup>-1</sup> K <sup>-1</sup> ]
$d_s$	Diameter of the solids [m]
$k_{ax}$	Axial heat transfer coefficient in the catalyst bed [W m <sup>-1</sup> K <sup>-1</sup> ]
$k_w$	Heat transfer coefficient in the wall [W m <sup>-1</sup> K <sup>-1</sup> ]
$k_i$	Kinetic constant of the reaction $i$
$n$	Apparent reaction order [–]
$r_i$	Radius [m]
$t$	Time [s]
$v_0$	Initial linear velocity [m s <sup>-1</sup> ]
$y_i$	Molar fraction [–]

### Capital letters

$A$	Reactor external surface [m <sup>2</sup> ]
$A_b$	Surface of a bubble [m <sup>2</sup> ]
$D$	Diffusion coefficient [m <sup>2</sup> s <sup>-1</sup> ]
$F_i$	Molar flow rate of the species $i$ [mol s <sup>-1</sup> ]
$H$	Reactor length [m]
$H_{GS}$	Heat transfer coefficient from the gas to the solid phase [W K <sup>-1</sup> m <sup>-2</sup> ]
$K_{GS}$	Mass transfer coefficient from the gas to the solid phase [mol m <sup>-2</sup> ]
$K_{eq}$	Equilibrium constant [–]
$K_i$	Adsorption coefficient
$R$	Universal gas constant [J mol <sup>-1</sup> K <sup>-1</sup> ]
$S_p$	Particle surface area [m <sup>2</sup> ]
$T$	Temperature [K]
$U$	Heat transfer coefficient [W m <sup>-2</sup> K <sup>-1</sup> ]
$V_p$	Particle volume [m <sup>3</sup> ]
$X_i$	Conversion of the species $i$ [–]
$Y_i$	Yield of the species $i$

### Adimensional numbers

$Nu$	Nusselt number [–]
$Pr$	Prandtl number [–]
$Re$	Reynolds number [–]

### Small greek letters

$\varepsilon_{bed}$	Bed porosity (considers the void volume in the bed) [–]
$\varepsilon_p$	Particle porosity (considers the void volume inside a particle) [–]
$\eta$	Catalyst effectiveness factor [–]
$\nu_{ij}$	Stoichiometric coefficient for the species $i$ in the reaction $j$ [–]
$\rho_i$	Density of the species $i$ [kg m <sup>-3</sup> ]
$\phi$	Thiele modulus [–]
$\mu$	Dynamic viscosity [Pa s]

### Capital greek letters

$\Delta H_j^R$	Reaction enthalpy in the reaction $j$ [J mol <sup>-1</sup> ]
----------------	--





## Conflicts of interest

The authors are employed by Hitachi Zosen Inova AG.

## Appendix

Fig. 11 reports the CH<sub>4</sub> concentration in the product SNG over the first 50 hours of operation of the reactor. The oscillations in the CH<sub>4</sub> concentration are mainly due to the change in the biogas composition.

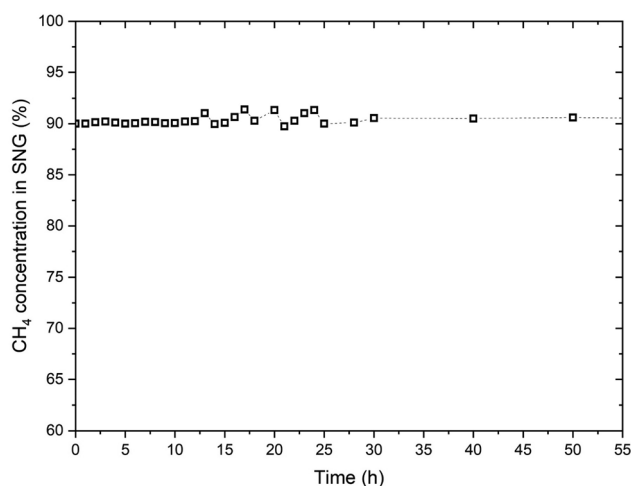


Fig. 11 The CH<sub>4</sub> concentration in SNG over the first 50 hours of operation of the reactor.

## Acknowledgements

The methanation reactor was installed in the project 'Renewable Gas Field – a demonstration project as part of the energy model region WIVA P&G' coordinated by Energie Steiermark AG. The project is funded by the Austrian climate and energy fund and runs within the scope of the program 'Vorzeigeregion Energie' (Funding institution: FFG, KPC Project number: 868849). The collaboration from the power-to-gas team of Hitachi Zosen Corporation (Japan) is gratefully acknowledged.

## References

- 1 S. Fogel, C. Yeates, S. Unger, G. Rodriguez-Garci, L. Baetcke, M. Dornheim, C. Schmidt-Hattenberge, D. Bruhn and U. Hampel, *Energy Adv.*, 2022, 402–421.
- 2 E. Panos, T. Kober and A. Wokaun, *Appl. Energy*, 2019, 252, 113470.
- 3 H. Nazir, N. Muthuswamy, C. Louis, S. Jose, J. Prakash, M. E. Buan, C. Flox, S. Chavan, X. Shi, P. Kauranen, T. Kallio, G. Maia, K. Tammeveski, N. Lymperopoulos, E. Carcadea, E. Veziroglu, A. Iranzo and A. M. Kannan, *Int. J. Hydrogen Energy*, 2020, 45, 20693–20708.
- 4 J. Gorre, F. Ortloff and C. van Leeuwen, *Appl. Energy*, 2019, 253, 113594.

- 5 S. Roussanaly, M. Vitvarova, R. Anantharaman, D. Berstad, B. Hagen, J. Jakobsen, V. Novotny and G. Skaugen, *Front. Chem. Sci. Eng.*, 2020, 14, 436–452.
- 6 I. Angelidaki, L. Treu, P. Tsapekos, G. Luo, S. Campanaro, H. Wenzel and P. G. Kougias, *Biotechnol. Adv.*, 2018, 36, 452–466.
- 7 M. Prussi, M. Padella, M. Conton, E. D. Postma and L. Lonza, *J. Cleaner Prod.*, 2019, 222, 565–572.
- 8 E. Moioli and T. Schildhauer, *Renewable Sustainable Energy Rev.*, 2022, 158, 112120.
- 9 J. Witte, A. Kunz, S. M. A. Biollaz and T. J. Schildhauer, *Energy Convers. Manage.*, 2018, 178, 26–43.
- 10 A. S. Calbry-Muzyka and T. J. Schildhauer, *Front. Energy Res.*, 2020, 8.
- 11 G. Leonzio, *Power to Gas Systems Integrated with Anaerobic Digesters and Gasification Systems*, Springer, Netherlands, 2019.
- 12 M. Burkhardt, T. Koschack and G. Busch, *Bioresour. Technol.*, 2015, 178, 330–333.
- 13 A. Gantenbein, O. Kröcher, S. M. A. Biollaz and T. J. Schildhauer, *Front. Energy Res.*, 2022, 9, 1–16.
- 14 P. Collet, E. Flottes, A. Favre, L. Raynal, H. Pierre, S. Capela and C. Peregrina, *Appl. Energy*, 2017, 192, 282–295.
- 15 B. D. Jønson, P. Tsapekos, M. Tahir Ashraf, M. Jeppesen, J. Ejbye Schmidt and J. R. Bastidas-Oyanedel, *Bioresour. Technol.*, 2022, 365, 128160.
- 16 E. Moioli, R. Mutschler, A. Borsay, M. Calizzi and A. Züttel, *Chem. Eng. Sci. X*, 2020, 8, 100078.
- 17 E. Moioli, *RSC Adv.*, 2022, 12, 10355–10365.
- 18 M. Specht and U. Zuberbühler, *Elem. Greenh. Gas Neutral Soc.*, 2013, 46.
- 19 R. Schlautmann, H. Böhm, A. Zauner, F. Mörs, R. Tichler, F. Graf and T. Kolb, *Chem. Ing. Tech.*, 2021, 93, 568–579.
- 20 M. Zavarkó, A. R. Imre, G. Pörzse and Z. Csödö, *Energies*, 2021, 14, 1–26.
- 21 M. Specht, J. Brelloch, V. Frick, B. Stürmer and U. Zuberbühler, in *Synthetic Natural Gas: From Coal, Dry Biomass, and Power-to-Gas Applications*, ed. T. J. Schildhauer and S. M. A. Biollaz, Wiley-VCH Verlag, 1st edn, 2016, pp. 191–220.
- 22 C. Dannesboe, J. B. Hansen and I. Johannsen, *React. Chem. Eng.*, 2020, 5, 183–189.
- 23 J. Witte, A. Calbry-Muzyka, T. Wieseler, P. Hottinger, S. M. A. Biollaz and T. J. Schildhauer, *Appl. Energy*, 2019, 240, 359–371.
- 24 J. Guilera, T. Andreu, N. Basset, T. Boeltken, F. Timm, I. Mallol and J. R. Morante, *Renew. Energy*, 2020, 146, 1301–1308.
- 25 T. Heller, in *Presentation at of the Biomass for Swiss Energy Future Conference*, Brugg, Switzerland, 2016.
- 26 D. Hafenbradl, in *Presentation at of the store & go final conference*, Karlsruhe, Germany, 2020.
- 27 Limeco, Media release Flagship project at Limeco in Dietikon: Inauguration of the first industrial power-to-gas plant in Switzerland, [https://www.powertogas.ch/wp-content/uploads/220429\\_Medienmitteilung\\_EN\\_Einweihung\\_PtG-Anlage.pdf](https://www.powertogas.ch/wp-content/uploads/220429_Medienmitteilung_EN_Einweihung_PtG-Anlage.pdf), (accessed 2 April 2023).



- 28 B. Kreitz, G. D. Wehinger and T. Turek, *Chem. Eng. Sci.*, 2019, **541**–552.
- 29 J. Riese and M. Grünewald, *Chem. Ing. Tech.*, 2020, **92**, 1887–1897.
- 30 F. Herrmann, M. Grünewald, T. Meijer, U. Gardemann, L. Feierabend and J. Riese, *Chem. Eng. Sci.*, 2022, **254**, 117632.
- 31 E. Moioli, N. Gallandat and A. Züttel, *Chem. Eng. J.*, 2019, **375**, 121954.
- 32 Awite Gas Analysis Systems General Data|AWIFLEX|AWIFLEX XL, [https://www.awite.de/wp-content/uploads/technical\\_data\\_sheet-awiflex-en-uk-10-rev14-04.pdf](https://www.awite.de/wp-content/uploads/technical_data_sheet-awiflex-en-uk-10-rev14-04.pdf), accessed 22 March 2023.
- 33 PEM Electrolyzer ME450\_H-TEC Systems products, <https://www.h-tec.com/en/products/detail/h-tec-pem-electrolyser-me-450/me450/>, accessed 24 March 2023.
- 34 H. Takano, Y. Kirihata, K. Izumiya and Y. Nishida, US2021275994A1, 2019.
- 35 F. Koschany, D. Schlereth and O. Hinrichsen, *Appl. Catal., B*, 2016, **181**, 504–516.
- 36 J. Xu and G. F. Froment, *AIChE J.*, 1989, **35**, 88–96.
- 37 C. H. Bartholomew, *Catal. Rev.*, 1982, **24**, 67–112.
- 38 ÖVGW, *RICHTLINIE GB210 Gasbeschaffenheit*, 2021.
- 39 A. Gantenbein, J. Witte, S. M. A. Biollaz, O. Kröcher and T. J. Schildhauer, *Chem. Eng. Sci.*, 2021, **229**, 116012.
- 40 E. Moioli and A. Züttel, *Sustain. Energy Fuels*, 2020, **4**, 1396–1408.
- 41 D. Schlereth and O. Hinrichsen, *Chem. Eng. Res. Des.*, 2014, **92**, 702–712.
- 42 K. L. Fischer, M. R. Langer and H. Freund, *Ind. Eng. Chem. Res.*, 2019, **58**, 19406–19420.
- 43 J. Bremer, K. Rätzer and K. Sundmacher, *AIChE J.*, 2017, **63**, 23–31.
- 44 K. L. Fischer and H. Freund, *Chem. Eng. J.*, 2020, **393**, 124722.
- 45 D. Sun, F. M. Khan and D. S. A. Simakov, *Chem. Eng. J.*, 2017, **329**, 165–177.
- 46 A. El Sibai, L. K. Rihko Struckmann and K. Sundmacher, *Energy Technol.*, 2017, **5**, 911–921.

